Highly photoactive TiO_2 microspheres for photocatalytic production of hydrogen

E. Pulido Melián[1*], M. Nereida Suárez[1*], T. Jardiel[2], D.G. Calatayud[2], A. del Campo[2], J.M. Doña Rodríguez[1], J. Araña[1], O. M. González Díaz[1]

[1]Grupo de Fotocatálisis y Espectroscopía para Aplicaciones Medioambientales (FEAM)- Unidad Asociada al CSIC por el Instituto de Ciencia de Materiales de Sevilla. Dpto. de Química. Instituto de Estudios Ambientales y Recursos Naturales (*i*-UNAT). Edificio Central del Parque Científico Tecnológico. Universidad de Las Palmas de Gran Canaria. Campus Universitario de Tafira. 35017 Las Palmas. Spain.

[2]Departamento de Electrocerámica, Instituto de Cerámica y Vidrio (CSIC), Kelsen, 5, 28049 Madrid, Spain

Corresponding authors: elisendapm80@hotmail.com (E. Pulido Melián), nereida.suarez.rodriguez@gmail.com (M. Nereida Suárez)

Abstract

In this study, the photocatalytic activity in hydrogen production of a TiO_2 catalyst with hierarchical structure and microsphere morphology was tested. This catalyst was synthesised by hydrolysis and condensation processes from a $Ti(OBut)_4$ precursor and calcined at 150ºC, 400ºC and 630ºC. Hydrogen production of the subsequent photocatalysts rose by two and three orders of magnitude after the incorporation of Au or Pt particles by photodeposition. The microspheres with and without metal modification were characterised by scanning electron microscopy-energy dispersive X-ray spectroscopy (SEM-EDX), X-ray diffraction (XRD), Raman, Brunauer–Emmett–Teller (BET) surface area, Fourier transform infrared spectroscopy (FTIR) and diffuse reflectance measurements. The highest production rates were obtained for the metal-modified photocatalysts calcined at 400ºC. Hydrogen production increased with Au loading, attaining a rate of 1118 $\mu mol \cdot h^{-1}$ for the 1.5wt% Au photocatalyst. However, the highest production rate in the case of Pt was attained with just 0.27wt% and was almost twice as high as that obtained with Au, 2125 $\mu mol \cdot h^{-1}$. When compared with previous studies by our team under the same conditions, this high production rate, obtained with a very low Pt loading, was only exceeded by the reference Aeroxide P25 TiO_2 catalyst with a Pt loading greater than 1.5wt%.

Keywords: TiO_2 microspheres, hydrogen production, photocatalyst, Pt, Au.

1. Introduction

The uncertainties generated by our energy dependence on non-renewable resources, as well as the rising awareness of the environmental impact when using such resources, have been the main driving force behind the development of alternative forms of energy [1-3]. In this respect, hydrogen has emerged as a potential energy carrier due to its high energy efficiency and pollutant-free combustion [4, 5]. However, to ensure sustainable hydrogen production changes need to be made with respect to the present situation in which most commercially-used hydrogen is obtained through the catalytic reforming and partial oxidation of fossil fuels. Alternative methods are gaining ground quickly in this respect. One of the most highly developed forms is the electrolysis of water using wind or solar generated electricity [6, 7], but expensive installation and operating costs are a major drawback. Although the efficiency rates remain very low, the most promising methods are photoelectrolytic water splitting and the generation of hydrogen from biomass using photobiological or enzymatic processes [8].

Photocatalysis is based on exciting the electrons of a semiconductor from the valence band to the conduction band generating electron-hole pairs. These pairs migrate to the surface giving rise to oxidation-reduction reactions with the water adsorbed on the surface and, hence, to the production of oxygen and hydrogen, respectively [9]. As the efficiency of this reaction is very low with current semiconductors, substances (normally organic) are normally incorporated in the suspension which are good reducing agents, and which are oxidised by direct hole capture or by hydroxyl radicals generated by water oxidation. The most commonly used reducing agents are alcohols like methanol, ethanol or propanol. Of these, and because of its high effectiveness, the model molecule for hydrogen production studies is methanol [10].

The most widely used semiconductor is TiO_2 due to its abundance, cost and chemical and photochemical stability. The hydrogen production activity of photocatalysts comprised only of TiO_2 is very low. One of the various modifications that can be made to the base TiO_2 to increase its activity is the incorporation of metal deposits that lower the electron-hole recombination rate. This also hinders back-reaction among the oxygen and hydrogen products since the points of the catalyst where the oxidation and reduction reactions are produced are physically separated [11-13].

In recent years, there has been a growing interest in the use of TiO_2 nanoparticles with hierarchical structures of, for example, solid or hollow sphere-, cocoon-, box-, flower- or sponge-like morphologies, which result from the assembly of nanobelts, nanorods, nanowires, nanoplates, nanospheres, spindle-like nanoparticles or nanocrystals. These hierarchical structures have high surface-volume ratios, retain a significant surface area with good crystallinity, reduce recombination possibilities as they promote electron-hole separation by increasing electron delocalisation, and in addition normally have micrometric dimensions which facilitate their separation by simple filtration [14-20].

Numerous studies have been published on the synthesis of hierarchical TiO_2, generally of hollow microspheres by templating or solvothermal methods [21]. In this respect, K. Yan and G. Wu published a recent review in which they compiled the different methods to obtain TiO_2-hollow microsphere based materials and the application of these materials in photocatalytic hydrogen production [22]. They describe how hollow microspheres have traditionally been obtained via templating synthesis, but that more and more works have considered template-free processes. The microspheres appear to be a type of structure which contributes to an increase in photocatalytic activity over nanoparticles as they favour carrier separation and light absorption. With a view to introducing improvements in the activity of this type of material, various studies have focused on enhancing the structure of the TiO_2 particles which make up the microspheres and on the incorporation of co-catalysts. In this respect, Z. Zheng et al [23] were able to modify the ratio of the facets {001}/{101} between 45% and 82%, finding that the optimum ratio for hydrogen production was 45%. Other studies have incorporated co-catalysts like, for example, Pt. K. Yan et al. [24] obtained materials with better hydrogen production rates than the commercial P25 catalyst with a 10wt% loading. In view of all the above, this present work focusses on the use of a TiO_2-based photocatalyst comprised of TiO_2 nanoparticles forming solid and not hollow microspheres for the photocatalytic production of hydrogen. One of the most important aspects in this work is that this photocatalyst requires no additive for its synthesis, which has been optimised in previous studies [25]. Basically, the solution of the titanium precursor in ethanol is subjected to a process of reflux and evaporation. The microspheres were subjected to different calcination temperatures and modified with Au and Pt surface deposits at different small loadings. All the resulting materials were tested in the optimised conditions of pH 5 and 25%vol methanol as determined in previous studies [26]. This enabled their comparison with the commercial photocatalyst,

Aeroxide P25 TiO_2. As well as being tested for hydrogen production, the synthesised photocatalysts were analysed with various characterisation techniques.

2. Methods and analytical techniques

2.1. Synthesis of the catalyst

The chemicals titanium (IV) tetrabutoxide ($Ti(OBut)_4$, 98%, Fluka, St. Louis, MO, USA) and anhydrous ethanol (EtOH, analytically pure, Merck, Whitehouse Station, NJ, USA) were used without further purification. The TiO_2 microspheres were obtained following a facile methodology previously developed by our team [25]. In short, a solution of $Ti(OBut)_4$ in 1 L of absolute ethanol was stirred at room temperature, and after 6.5 h evaporated to dryness under atmospheric conditions. The evolved white precipitate was washed thoroughly with distilled water and anhydrous ethanol and then dried at room temperature. A yield of over 97% was attained. The powder thus obtained was spread on a high-density alumina crucible and further subjected to a firing step at 150ºC for 24 h, 400ºC for 1 h, and 630ºC for 1 h (heating rate of $1ºC \cdot min^{-1}$).

2.2. Metal photodeposition

For metal photodeposition (Au and Pt), a modification was used of the method described by Hufschmidt [27]. Ultrapure Milli-Q water, *2*-propanol (Panreac >99.8%) and the catalyst were added to an immersion reactor and subjected to constant stirring (photochemical reactor). A flow of N_2 was then introduced to displace the dissolved oxygen, which was maintained throughout the process. The desired amount of metal for catalyst photodeposition was added after ten minutes from a chloroplatinic acid hexahydrate solution (~40% Pt Sigma-Aldrich) or a gold chloride trihydrate solution (≥99.9% Sigma-Aldrich). Illumination was then initiated for 6 h using a medium-pressure 400 W mercury lamp placed inside a water-cooled quartz jacket. After the photodeposition process, the catalyst was separated by filtration. The deposits are expressed in wt% as in (weight metal/weight TiO_2)·100.

2.3. Activity test

The system used for the activity test was the same as described in reference [28]. The system was comprised of a borosilicate reactor to which was added 200 mL of a 25%vol aqueous suspension in methanol with a 1 $g \cdot L^{-1}$ photocatalyst concentration and adjusted to pH 5 by means of an NaOH solution. The reactor was subjected to constant stirring at

700 rpm. Two Solarium Philips HB 175 lamps were used as illumination source, each equipped with 4 x 15W Philips CLEO fluorescent tubes with a radiation spectrum from 300 to 400 nm (maximum at 365 nm). Before illumination, the reactor was purged with nitrogen and, during the tests, a continuous flow of 5 $mL \cdot min^{-1}$ was maintained through the reactor headspace which carried the generated hydrogen to a chromatograph. The hydrogen signal was recorded each 30 min for 8 h using a Shimadzu 2010 gas chromatograph equipped with TCD detector and MolSieve 5A column. The suspension was filtered after conclusion of the test. In liquid phase, the concentration of formaldehyde was determined by a spectrophotometric method [29], and of formic acid by high resolution liquid chromatography using a Varian ProStar device equipped with a diode array UV-Vis detector (Supelcogel column, H_3PO_4 1%vol phosphoric acid in water, 1 $mL \cdot min^{-1}$, 25ºC).

2.4. Characterisation techniques

The analyses of crystalline structure and phase identification were performed by X-ray diffraction (XRD Bruker D8 ADVANCE, Madison, WI, USA) with a monochromatized source of Cu-Kα1 radiation (λ = 1.5406 nm) at 1.6 kW (40 KV, 40 mA); samples were prepared by placing a drop of a concentrated ethanol dispersion of particles onto a single crystal silicon plate. Crystal sizes of the different phases were estimated from line broadening of the corresponding X-ray diffraction peaks by using the Scherrer equation. Anatase–rutile semi-quantitative fractions were calculated taking into account the relative diffraction peak intensities of crystalline planes [1 0 1] and [1 1 1] of anatase and rutile, respectively.

Field emission scanning electron microscopy was carried out on a Hitachi S-4700 Cold-FESEM working at 20 kV.

The specific surface area was determined by the Brunauer-Emmett-Teller (BET) method in a Monosorb Analyzer MS-13 QuantaChrome (Boca Raton, FL, USA).

Raman spectra were obtained using a micro-Raman system with a 532 nm excitation laser (maximum power output 50 mW) through a 100X objective (N.A. 0.95). The incident laser power was fixed at 1 mW to avoid possible undesirable sample modifications. The Raman images of 30x30 microns consisted of 3600 spectra of 0.3 seconds of integration time each. The collected spectra were then analysed using the Witec Control Plus Software (Witec, Ulm, Germany), fitting Raman mode positions to Lorentzian functions.

Transmission infrared spectra were acquired by a Thermo Scientific-Nicolet iS10 spectrophotometer at 2 cm^{-1} spectral resolution. The catalysts were placed between two CaF_2 mirrors and their spectra recorded in a 4000-1000 cm^{-1} range.

UV-Vis diffuse reflection spectra (DRS) were obtained using a Varian Cary 5 spectrophotometer, and the reflection data were converted to absorbance through the standard Kubelka–Munk method [30, 31]. Tauc's method for allowed indirect transitions was applied to calculate the band-gap energy values [32].

3. Results and discussion

3.1. Microsphere calcination temperatures

The structural characteristics of the microspheres calcined at different temperatures are shown in Table 1, along with those of the Aeroxide P25 TiO_2 photocatalyst for comparison purposes.

Table 1

Characteristics of the microspheres calcined at different temperatures and of the Aeroxide P25 TiO_2.

photocatalyst	%anatase	%rutile	anatase crystal /nm	rutile crystal /nm	BET surface/ $m^2 \cdot g^{-1}$	pore volume/ $cm^3 \cdot g^{-1}$	band gap/ eV	Average microsphere diameter / μm
M150	100	0	3.6	-	196.36	0.2089	3.18	1.25
M400	100	0	9.3	-	77.52	0.0681	3.15	1.75
M630	75	25	46.9	73.4	1.09	0.0048	2.98	1.75
P25	79	21	23	44	48.6	0.1760	3.18	-

The following calcination temperatures were selected: (i) a low calcination temperature, 150ºC, at which the catalyst retains a high specific surface area and some crystallinity has developed according to the XRD pattern (Figure 1A). In this case, the temperature was so low that 1 hour was insufficient to properly remove all the solvents (butanol, ethanol and water) from the synthesis stage, and so the annealing time was increased to 24 hours; (ii) a moderate calcination temperature, 400ºC, at which the microspheres display an anatase structure with some crystallinity, and; (iii) a higher calcination temperature, 630ºC, at which the microspheres have a low percentage of rutile phase

accompanying the anatase. This rutile phase percentage is very similar to that found in the reference photocatalyst, the Aeroxide P25 TiO_2 (P25), whose high activity is explained by an anatase:rutile phase ratio of around 80:20 which results in a better electron-hole separation [33, 34].

Figure 1

(A) XRD profiles and (B) pore volume distribution for microspheres calcined at different temperatures.

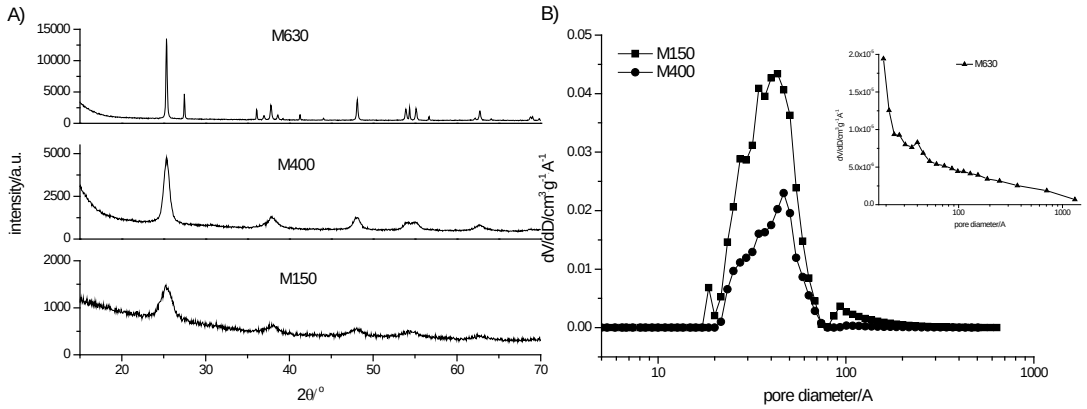

The morphology of the particles is one of nanostructured microspheres of approximately 1-4 microns in diameter comprised of self-assembled nanoparticles (Figure 2). For the M150 catalyst, treated at the lowest temperature, the average diameter was 1.25 microns. This value was slightly higher, 1.75 microns, for the M400 and M650 catalysts, due to the higher temperatures used in the corresponding thermal treatments which led to a slight growth of the spheres (Figure 2). This is within the average 1-8 micron size reported in the literature for TiO_2 microspheres [35-37]. The Raman signal magnitudes found in the microparticles are quite high, indicating the nanometric nature of the particles which make up the microspheres [38] (Figure 9). Increases in calcination temperature did not result in alterations to microsphere morphology or size, but changes in specific surface area were observed. An important decrease in mesoporosity can be seen in Figure 1B as temperature increases, although the shape of the distribution remains centred around 4 nm for the M150 and M400 catalysts. Porosity of the catalyst calcined at 630ºC was virtually eliminated and its specific surface area fell to 1.09 $m^2 \cdot g^{-1}$.

Figure 2

FE-SEM micrographs and sphere size distribution of a) M150, b) M400 and c) M630.

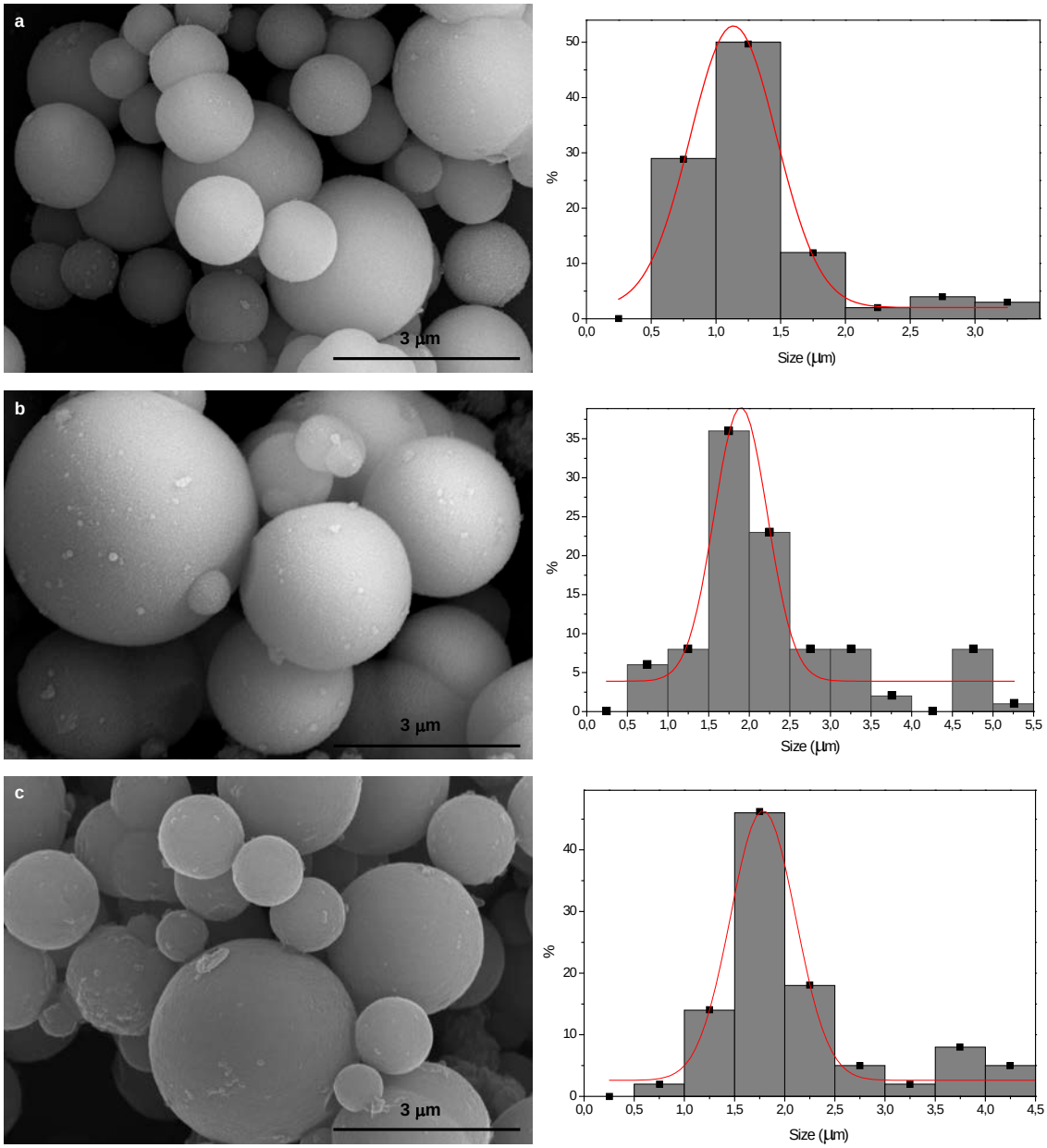

The hydrogen production rates of these photocatalysts are shown in Figure 3. The production rates increase over time until reaching the highest production rate which remained stable until the 8 h of the test had concluded (steady-state rate). The low porosity and important decrease in specific surface area could explain the very low hydrogen production of the M630, 0.79 µmol·h^{-1}, despite having an anatase:rutile phase ratio to which many authors attribute the high activity of P25 [34]. The M400 catalyst attained a hydrogen production rate of 6.51 µmol·h-1, higher than the 4.0 µmol·h^{-1} rate

of the P25 and, surprisingly, the M150 attained a very high production rate, 24.64 $\mu mol \cdot h^{-1}$ (2.6% quantum efficiency), much higher than the values reported for unmodified commercial nanoparticulated TiO2 catalysts tested in similar conditions [39]. This production rate was 6 times greater than that obtained for the P25. There appears to be a clear correlation between specific surface area and hydrogen production rates for these photocatalysts without metal surface modification.

Figure 3

Hydrogen production patterns of the M150, M400 and M630 microspheres.

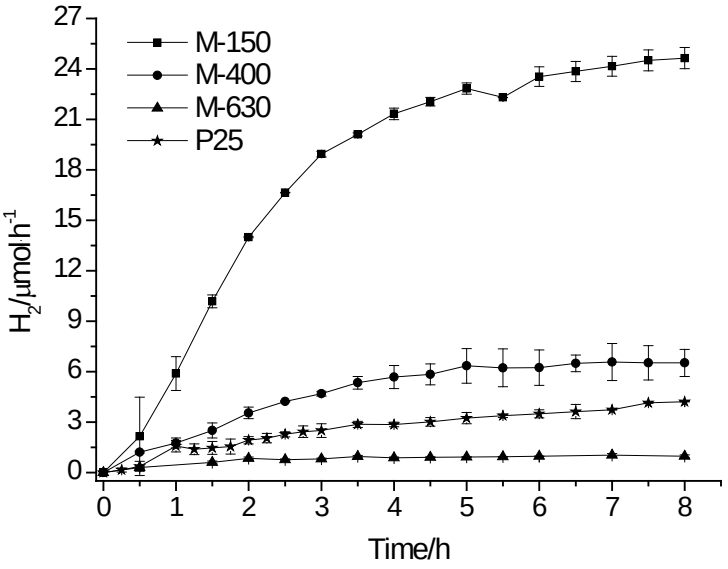

With a view to obtaining a better understanding of the possible reasons for this correlation, Fourier-transform infrared spectrophotometry (FTIR) was used for surface characterisation.

The FTIR spectra of the catalysts are shown in Figure 4. A correlation can be seen between the activities and the baseline positions. The baseline increase in some catalysts has been correlated with the presence of shallow electron traps [40-43]. The highest baselines were recorded in the M630 and M400, indicating that these catalysts, especially the M630, have a higher abundance of this type of trap. Their intense presence is usually associated with an important inhibition of the interaction of the water with the surface and, therefore, there was no detectable evidence for these catalysts of surface hydration after contact with the reaction medium.

The role played by the water is extremely important in these hydrogen production photocatalytic processes in the presence of a sacrificial agent like methanol and in anaerobic conditions. However, its importance is not so much as a hydrogen ion supplier, but rather as a vehicle which transports these ions from the methanol to the sites where the photoelectrons are found trapped in the conduction band or the shallow electron traps [44, 45]. Bahruji et al. [44] established some general rules to determine which reaction intermediates are produced in the catalytic photoreforming depending on the alcohol used as sacrificial agent. The first of these rules states that the alcohol must have hydrogen atoms on the *C* attached to the alcohol group.

In these [44, 45] and other studies [46], it has been confirmed that the first step in the hydrogen production catalytic photoreforming process, apart from the photoexcitation of the semiconductor, is the capture of the photogenerated hole by the methanol. Adsorption of the methanol takes place even in the dark and is usually dissociative. Under UVA irradiation and anoxic conditions, the transfer of electrons from the alcohol (methoxy groups) to the holes is favoured, causing a stabilising effect for the photogenerated electrons present in the conduction band, as well those in the traps [46]. So, the baseline increase of the catalysts after entering into contact with the reaction medium must be considered clear evidence of adsorption of the methanol on the photocatalyst (Figure 4). This effect occurs intensely in the M150 and the P25, negligibly in the M400 and inversely in the M630. This behaviour appears to be related, according to [46], with the porosity of the material. Such a correlation could explain what was seen in the FTIR interferograms for the M150 microspheres (with the highest pore volume, 0.2089 $cm^3 \cdot g^{-1}$), namely a significant baseline increase which indirectly indicates the dissociative methanol adsorption in the photogenerated holes on the TiO_2 surface under the experimental conditions. At the same time, no baseline increase is observed in the case of the M400 (0.0681 $cm^3 \cdot g^{-1}$), while an opposite effect is found with the M630 where the microsphere can be considered practically smooth (0.0048 $cm^3 \cdot g^{-1}$). The adsorption of the methanol and the subsequent reaction, in this latter case, not only does not provoke the expected baseline increase but actually results in its decrease. This consumption of shallow-trapped electrons, which only occurs clearly in the M630, could be related to an increase of the recombination stages between surface-trapped photogenerated pairs, reactions (5) and (6) described below. All this would appear to be clearly correlated to the extremely low surface hydroxylation, low

methanol adsorption, low specific surface area and almost null pore volume of the M630.

In the case of the P25, the reference catalyst in this study, pore volume is practically the same as that of the M150, and so, after adsorption of the methanol and in the same experimental conditions as the other catalysts, a baseline increase is also produced. This situation has also been seen, for the P25, in FTIR adsorption studies of water [47]. These authors also correlate the dissociative rupture of the water molecule with the increase and stabilisation of the surface-trapped electrons, and so a baseline increase in the FTIR interferograms of the TiO_2 with adsorbed water is also found. In the case which concerns us, the reaction medium contains mostly water and, logically, the water as well as the methanol will participate in this type of adsorption, whether molecular or dissociative, provoking the corresponding baseline increases.

Figure 4

FTIR spectra of the catalysts before and after reaction.

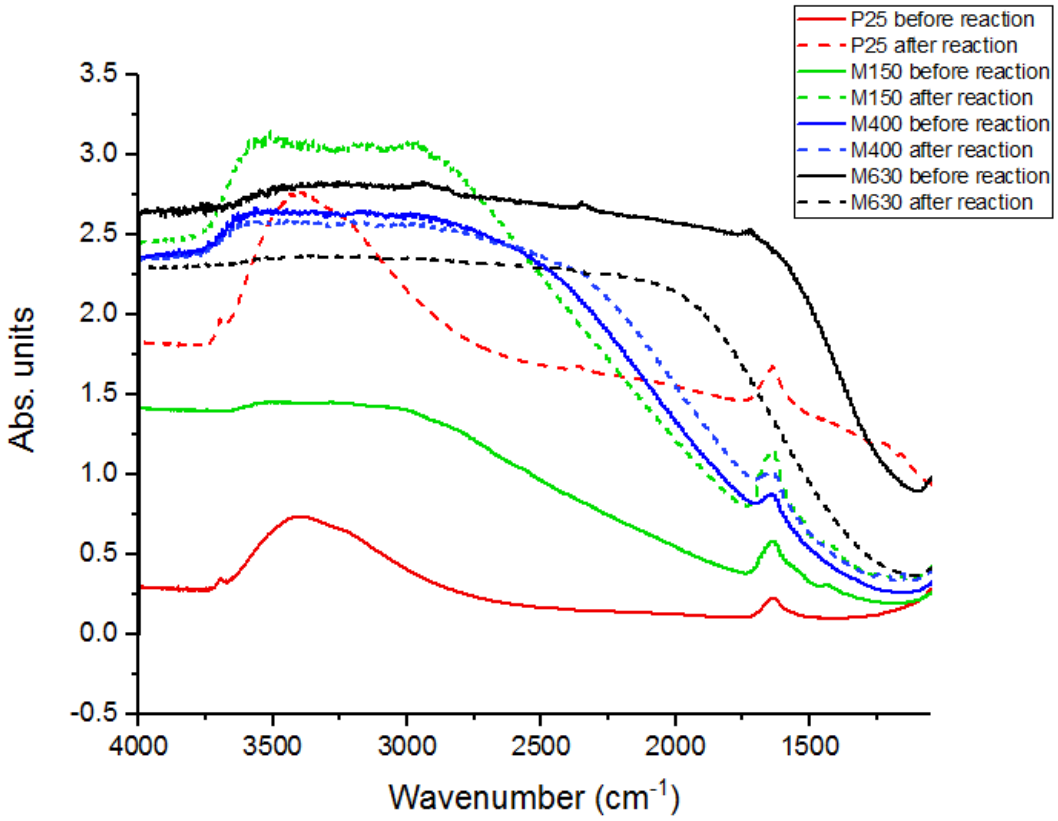

However, the greater hydrogen production of the M150 compared to the P25 is due to a number of reasons:

- The higher specific area and slightly larger pore volume of the M150.

- The larger particle size of the M150 compared to the P25 (microns vs. nanometres) means that the former will have a larger exposed area to the reaction medium for each particle. This will enable greater hydration and interaction with the sacrificial agent, as clearly seen in the post-reaction interferogram for this photocatalyst (Figure 4) with the increase in the baseline (dashed green line).

- Water and methanol adsorption appears to be more intense in the M150. This adsorption can be observed in the greater broadening of the bands that can be seen in Figure 4 (between 2700-3550 cm^{-1}). These bands are associated to physisorbed water [48] and in this same region are found some of the characteristic bands of methanol which could be masked by those of the water, especially in this region of high frequencies (ν_{OH} 3550 cm^{-1} and $\nu_{as}CH_3$ and $\nu_{s}CH_3$ 2950 and 2840-2850 cm^{-1}, respectively) [49].

The reactions involved in this process for unmodified TiO_2-based photocatalysts in the absence of a sacrificial agent have been described by numerous authors, most notably S. H. Szczepankiewicz et al. [41]. They established that, once the photoexcitation of the semiconductor has been produced, the photogenerated charges can be trapped on the hydroxylated surface of the TiO_2:

$$TiO_2 + h\nu \longrightarrow e^- + h^+ \quad (1)$$

$$e^- + Ti(IV)OH \longrightarrow Ti(III)OH^- \quad (2)$$

$$h^+ + Ti(IV)OH \longrightarrow Ti(IV)O^{\bullet}H^+ \quad (3)$$

Reactions (2) and (3) correspond to electron and hole traps, respectively, on the hydroxylated TiO_2 surface. Other described reactions which can take place are the formations of oxygen vacancies, V_o, which, in turn, produce adsorbed oxygen. This reaction (4) could be produced as the result of the interaction of lattice oxygens with photogenerated holes. Reactions (5) and (6) correspond to recombination processes between photodissociated pairs.

$$h^+ + \frac{1}{2}O^{2-} \longrightarrow \frac{1}{4}O_2 + V_O \quad (4)$$

$$h^+ + Ti(III)OH^- \longrightarrow Ti(IV)OH \quad (5)$$

$$e^- + Ti(IV)O^{\bullet}H^+ \longrightarrow Ti(IV)OH \quad (6)$$

Reaction (3) also corresponds to the presence of surface hydroxyl radicals. When a primary alcohol is used as sacrificial agent, it is the alcohol which acts as principal hole scavenger and enters into direct competition with reactions (3) and (4) which involve the holes photogenerated through (7). This reaction, as previously mentioned, has been described by numerous authors [35-37]:

$$CH_3OH + h^+ \longrightarrow CH_3O^{\bullet} + H^+ \quad (7)$$

The methoxy radical that is produced can continue interacting with the photogenerated holes and, according to [45], freeing hydrogen ions and capturing holes, to transform into adsorbed formaldehyde:

$$CH_3O^{\bullet} + h^+ \longrightarrow H_2CO + H^+ \quad (8)$$

The adsorbed formaldehyde formed through (8) can transform into CH_2OO (formic acid) [50], which can continue transforming in subsequent stages to formate species which decompose to CO_2 and carbonate species. These stages consume holes and

generate hydrogen ions. The hydrogen ions with the surface electrons will produce hydrogen:

$$2H^{+} + 2Ti\left(III\right)OH^{-} \longrightarrow H_2 + 2Ti\left(IV\right)OH \quad (9)$$

Stages (7) and (8), and those which give rise to the formation of formate species, have been confirmed in the present study, given that both formaldehyde and formic acid were detected, in the suspension, after the reaction. These photogenerated-hole consumption processes inhibit the recombination stages (5) and (6) and, therefore, favour hydrogen production. This hydrogen production is dependent on the morphological-textural characteristics and the particle size of the unmodified photocatalysts, as seen in Table 1 and in the images presented in Figure 2.

3.2. Incorporation of Pt and Au

As has been seen, significant hydrogen production rates were not obtained with the unmodified photocatalysts, although they were higher with the M150 and M400 microspheres than the P25 commercial photocatalyst. It is known that the addition of noble metals, in an optimal proportion on the TiO_2 surface, can have various positive effects which increase production. Their incorporation decreases photogenerated-pair recombination, reactions (5) and (6), as they act as electron scavengers, and moreover lower the overpotential for hydrogen formation on the TiO_2 surface. If, in addition to these positive effects, the presence is added of a sacrificial agent which acts as a hole scavenger, the recombination rate of the photodissociated pairs diminishes considerably. All this takes place in the absence of oxygen, as the oxygen competes more efficiently for the electrons than the hydrogen ion [12, 13]. The different stages presented above (reactions 1-9) have different time scales, with photodissociation occurring in *fs* and recombination between 10 and 100 *ns*. Direct reduction through the electrons requires longer times, *ms*, while the reactions of direct oxidation by holes are in the order of 100 *ns* [51]. The electrons therefore need to be maintained for a longer time, which is achieved by trapping them with the help of metal nanoparticles. When a metal with an appropriate work function value is deposited on the surface of a semiconductor, the generated photoelectrons migrate to the metal. The Schottky barriers, which form on the metal-semiconductor interface, act as an efficient photogenerated-electron trap which impedes recombination. The electrons, trapped on the metal particles, reduce the hydrogen ions to hydrogen gas [51].

The noble metals chosen for the present study to increase hydrogen productivity were Pt and Au.

Figure 5.

Hydrogen production of the Pt- and Au-modified photocatalysts.

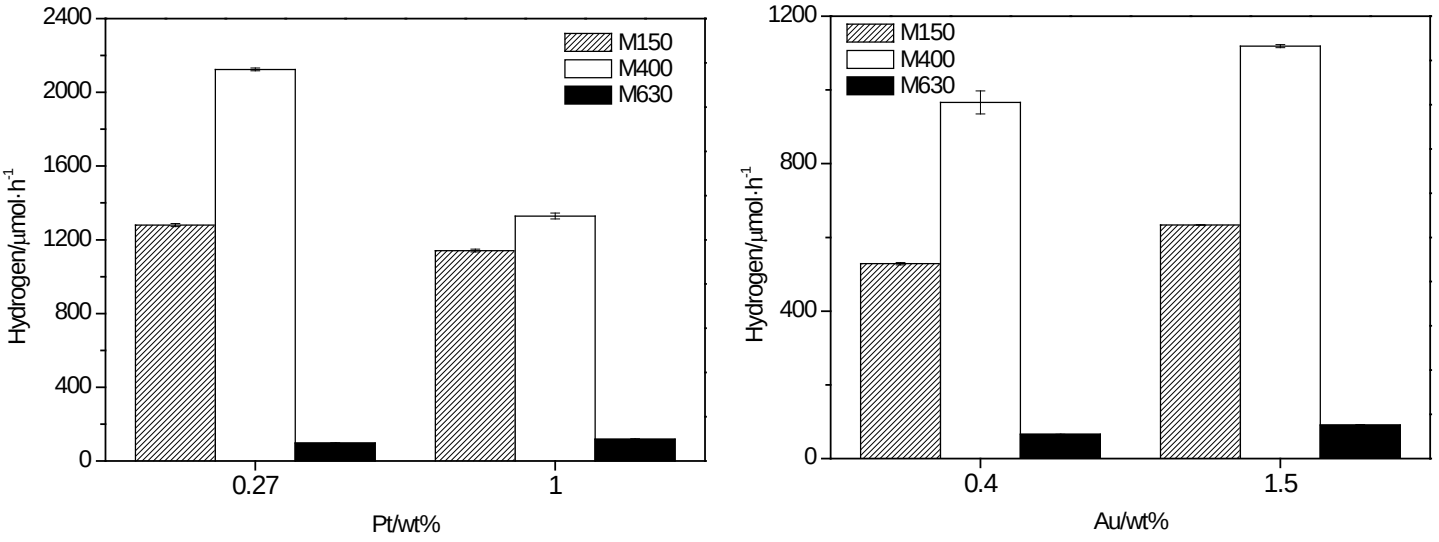

Figure 5 shows the results of the hydrogen production photoactivity tests of the M150, M400 and M630 microspheres modified with metal deposits. It can be seen that although the M150 gave the highest production when no metal deposits were present, in this case higher activities were obtained with the M400 than the M150 or M630.

With a view to understanding the effect produced by the particles of these metals on the TiO_2 surface, an analysis was conducted using FTIR interferograms.

In Figure 6A, it can be seen that the effect of Pt photodeposition was not the same for the various microspheres. In the M400, a decrease of the baseline of the infrared spectrum is observed after metal deposition, which is more significant again in the M630. This would seem to indicate that a transfer is taking place of the electrons present in the TiO_2 traps to the empty 5*d* orbitals of the Pt. This baseline decrease is accompanied by complete dehydration in the case of the M630, which does not happen so intensely in the case of the M400 where the water band is detectable albeit with lower intensity. Contrastingly, with the M150, it can be seen that metal deposition

produces a baseline increase; in other words, it appears that in this case a transfer takes place of the electrons of occupied orbitals of the Pt to the *d* orbitals of the TiO_2. This effect may be due to a possible influence of the clearly different surface parameter characteristics for these materials (Table 1). A lower specific area, as with the M400 and M630, can more efficiently aggregate the nanoparticles of the metal, giving rise to larger-sized clusters. This could explain the transfer of electrons from the shallow thermal traps to the metal clusters. The clear difference in the nature of the surface of these materials could explain why the interaction of the metal with the TiO_2 microsphere is different and, hence, a different effect on the photocatalytic process would be expected. In the case of the P25, a decrease has been described of the adsorption of methanol when this commercial photocatalyst is modified with Pt [45]. The authors attributed it to the tendency of the metal particles to deposit and grow in oxygen vacancies, which are the active sites where it is believed the dissociative adsorptions are preferentially produced of both the water and the sacrificial agent, the methanol. The growth of these metal particles in these sites (nucleation centres of metal clusters) is therefore a determining factor in the decreased adsorption of the sacrificial agent, observed in the P25. In this respect, the question of the nanometric size of the P25 as opposed to the micrometric size of the microspheres should also be considered. In the latter, all the vacancies are not occupied when the material is surface modified with metals. This was verified in the modified M400 in the Raman characterisation described below. The decrease in intensity of the water bands in the FTIR interferograms is therefore also associated with this increase of metal particles in such active centres [12, 13]. In the present work, this effect is markedly observed in the sample calcined at the highest temperature, the M630. However, in the FTIR interferograms of the M150 and M400 samples (Figure 6A) the complete loss is not observed of the bands which correspond to surface adsorption of the water and, possibly, those of the metal would also not disappear completely, though these would be masked by the bands of adsorbed water [48, 49].

In the case of photodeposition with Au (1.5wt%), the behaviour was similar to that with Pt. In the M150, the surface Au aggregates or nanoparticles transfer electrons to the shallow electron traps (baseline increase of the corresponding interferogram) and favour the presence of adsorbed water. Contrastingly, for the M400 and M630 catalysts, a transfer of electrons takes place from the shallow electron traps to the metal particles which provokes the baseline decrease seen in the corresponding interferograms, with the

decrease more intense for the case of the sample calcined at 630 °C, the M630. Again, a complete loss is observed in the intensity of the bands assigned to water in the case of the M630, as is a significant loss in the case of the M400, which is in accordance with a greater occupation of the active centres of the dissociative adsorption of the water on the part of the Au clusters. The latter does not take place in the case of the M150, where an important increase is observed in the intensity of the bands assigned to adsorbed water, probably due to the greater pore volume and specific surface area.

Figure 6

FTIR spectra of the catalysts with and without photodeposited metals. Pt (A) and Au (B).

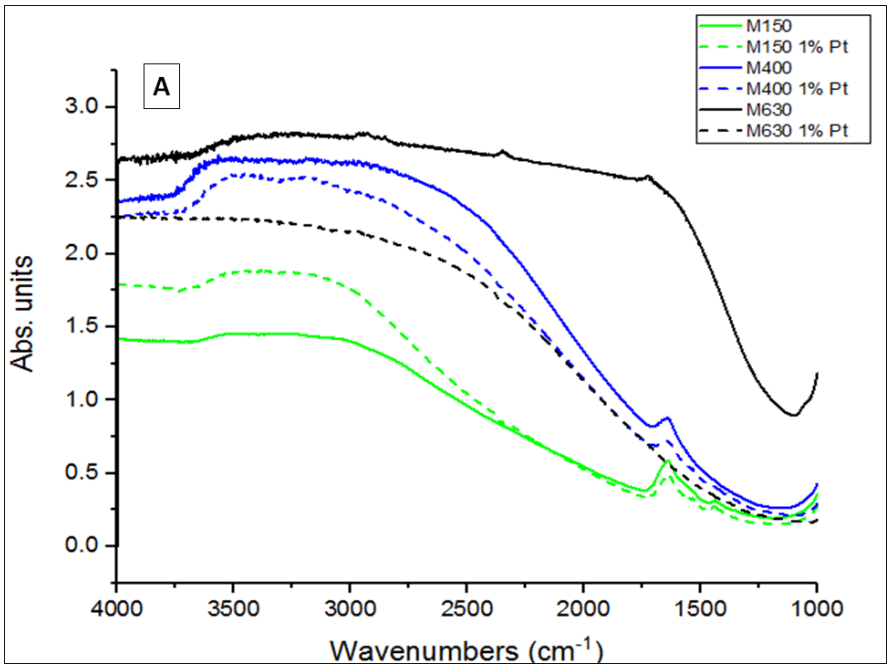

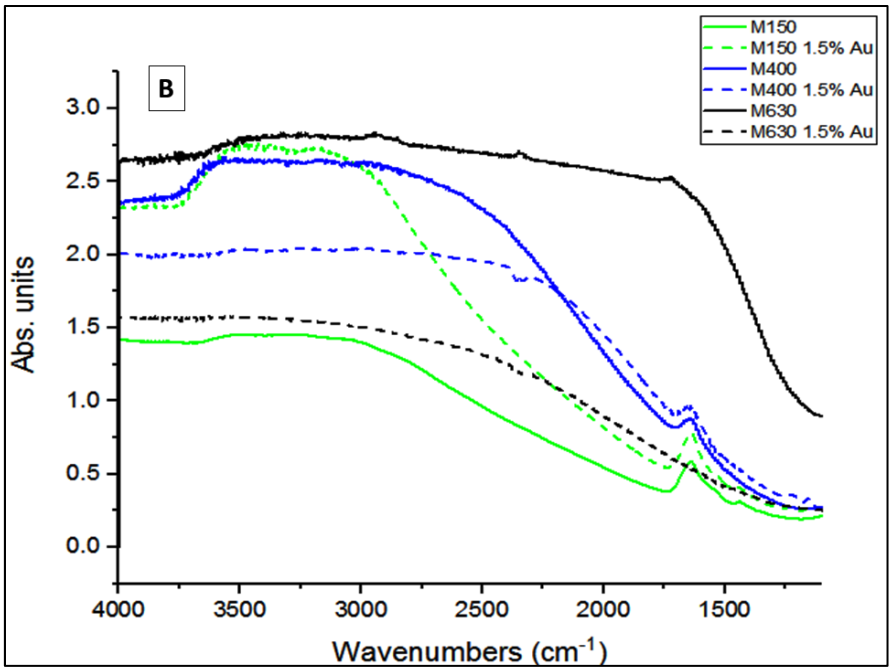

3.2.1. M400

Figure 7

Hydrogen production of the Pt (A) and Au (B) modified M400 photocatalyst.

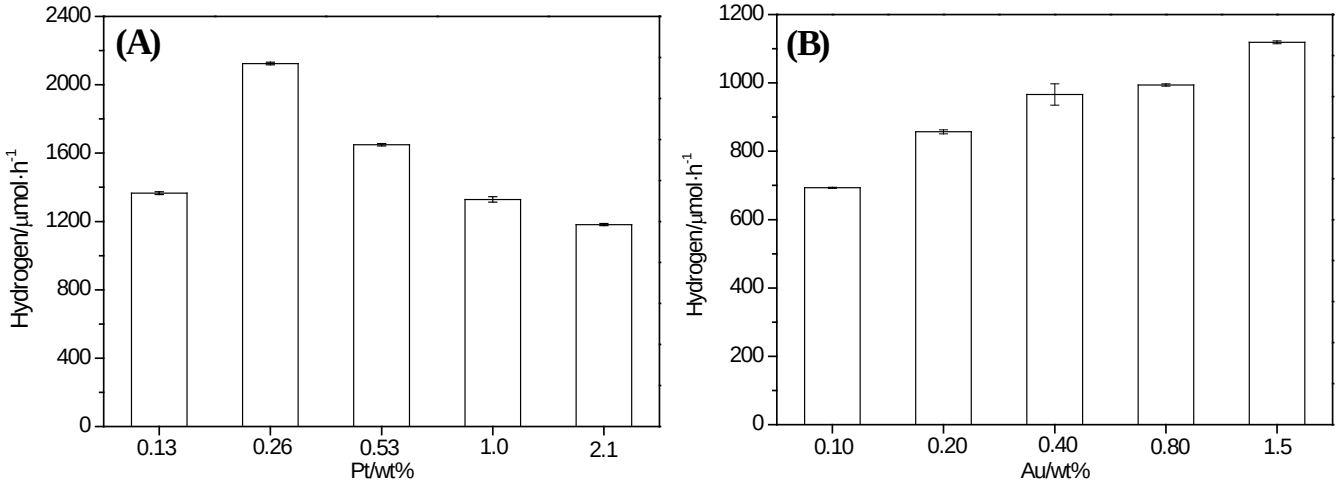

As the M400 photocatalyst gave the highest hydrogen production levels, this photocatalyst was selected to undertake a more in-depth analysis of the effect of different metal percentages. Figures 7 A and B show the hydrogen production rates for the M400 catalyst with different Pt and Au loads, respectively.

In the case of surface-modified photocatalysts with Pt or Au metal nanoparticles, there is an optimal metal percentage weight beyond which hydrogen production no longer increases or even falls significantly. This decrease has been attributed in the literature to the increase in Rayleigh scattering (opacity of the suspension) [12], or to other factors such as generation by the metal particles of disperse recombination centres on the surface or impedance by the metal particles of sacrificial agent adsorption [13].

For Pt, within the interval studied, the production rate was observed to rise and then fall, with the highest rate of 2124 $\mu mol \cdot h^{-1}$ obtained at just 0.27wt%. In the case of Au, it was observed that microsphere activity increased with the content of this metal. A production rate of 693 $\mu mol \cdot h^{-1}$ was obtained for 0.1wt%, and of 1118 $\mu mol \cdot h^{-1}$ for 1.5wt%. Results previously obtained by our team for the P25 [12] show that its hydrogen production was significantly lower than the production rates obtained in the present study with the Au-modified nanospheres. The maximum hydrogen production obtained for the P25 was 364 $\mu mol \cdot h^{-1}$ at 0.4wt% of Au, almost four times lower than that obtained in the present study with the M400 microspheres. Although a maximum hydrogen production was not attained in the studied Au range, it was decided not to continue increasing the Au load given that it would not be cost effective to increase the synthesis costs when the hydrogen production rates attained with low Pt percentages were not going to be reached with Au.

Attaining such a high production rate with such a low Pt percentage was surprising, as the optimum Pt percentages are normally in the order of 1.0wt% or higher [13, 15]. This is the case of the Aeroxide P25 TiO_2 which, to achieve a similar production rate, required 1.0wt% of Pt according to previous studies by our group [13].

Hydrogen production rates were higher for Pt than for Au, which was in accordance with the intermediate concentrations of methanol oxidation observed in both cases. Formaldehyde concentrations were between 60-115 mM for M400-Pt and 34-72 mM for M400-Au, and formic acid concentrations between 0.2-0.9 mM and below 0.34 mM, respectively. The detection of these intermediates is in accordance with reactions (7) and (8) and, of course, with those that follow down to the formation of formate species and their subsequent decomposition to CO_2 and carbonate species.

Incorporation of these metals on the surface did not result in any modification to the morphology of these TiO_2 microspheres (Figure 8) nor, according to the XRD analysis, to the crystalline structure (Figure 9). All diffraction maxima correspond to TiO_2

anatase (ICDD file no. 21-1272), except those marked corresponding to platinum and gold and which were confirmed by XPS (Supporting Information).

Figure 8

FE-SEM micrographs of a) M400, b) M400-0.27% Pt and c) M400-0.4% Au.

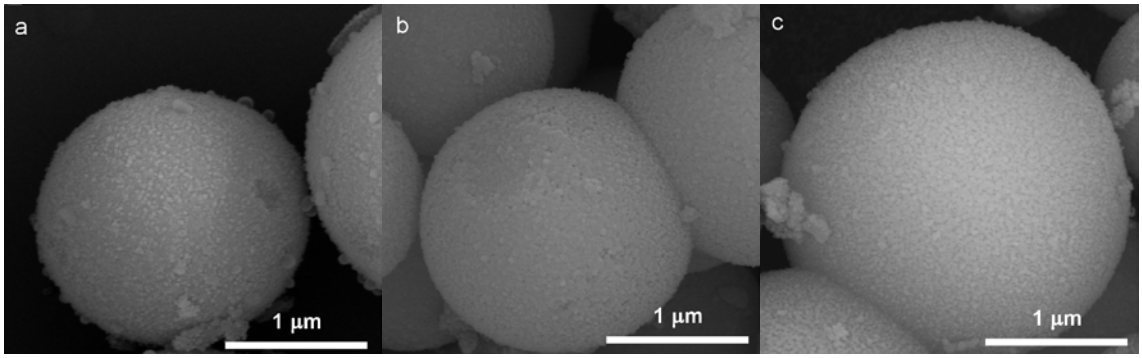

Figure 9

XRD patterns of the powders M400 (curve a) M400-2.1% Pt (curve b), and M400-1.5% Au (curve c).

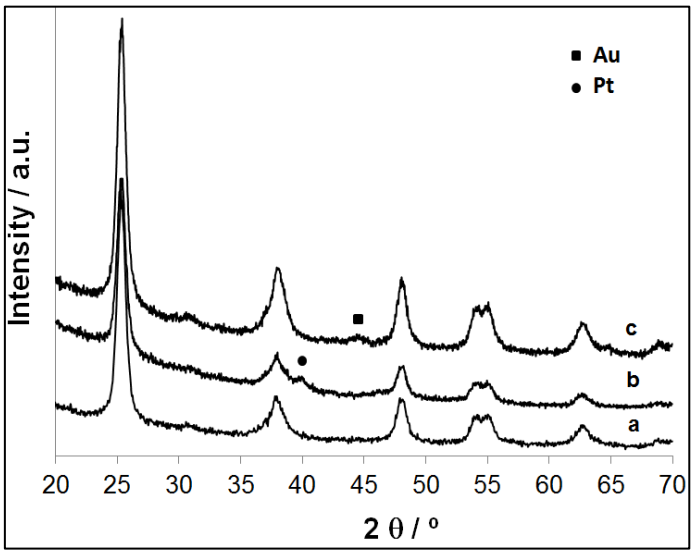

However, the Raman spectra (Figure 10) of the M400 catalysts with the highest Pt and Au content showed that some microspheres had rutile phase, though only slightly crystalline. In addition, it was observed that as metal content increased the main vibration band of the E_g 144 cm^{-1} anatase mode widened and shifted to lower wavenumbers in a similar way for both metals (Figure 10 C).

Figure 10

A and **B:** Raman spectra of the different M-400 based photocatalysts. The inserts show the spatial phase distribution of the samples with the highest metal content percentage (the blue region corresponding to rutile and the red to anatase); **C:** Raman shift and FWHM corresponding to the anatase main peak at 144 cm^{-1} (E_g mode) for the different photocatalysts as a function of metal content.

A) and B)

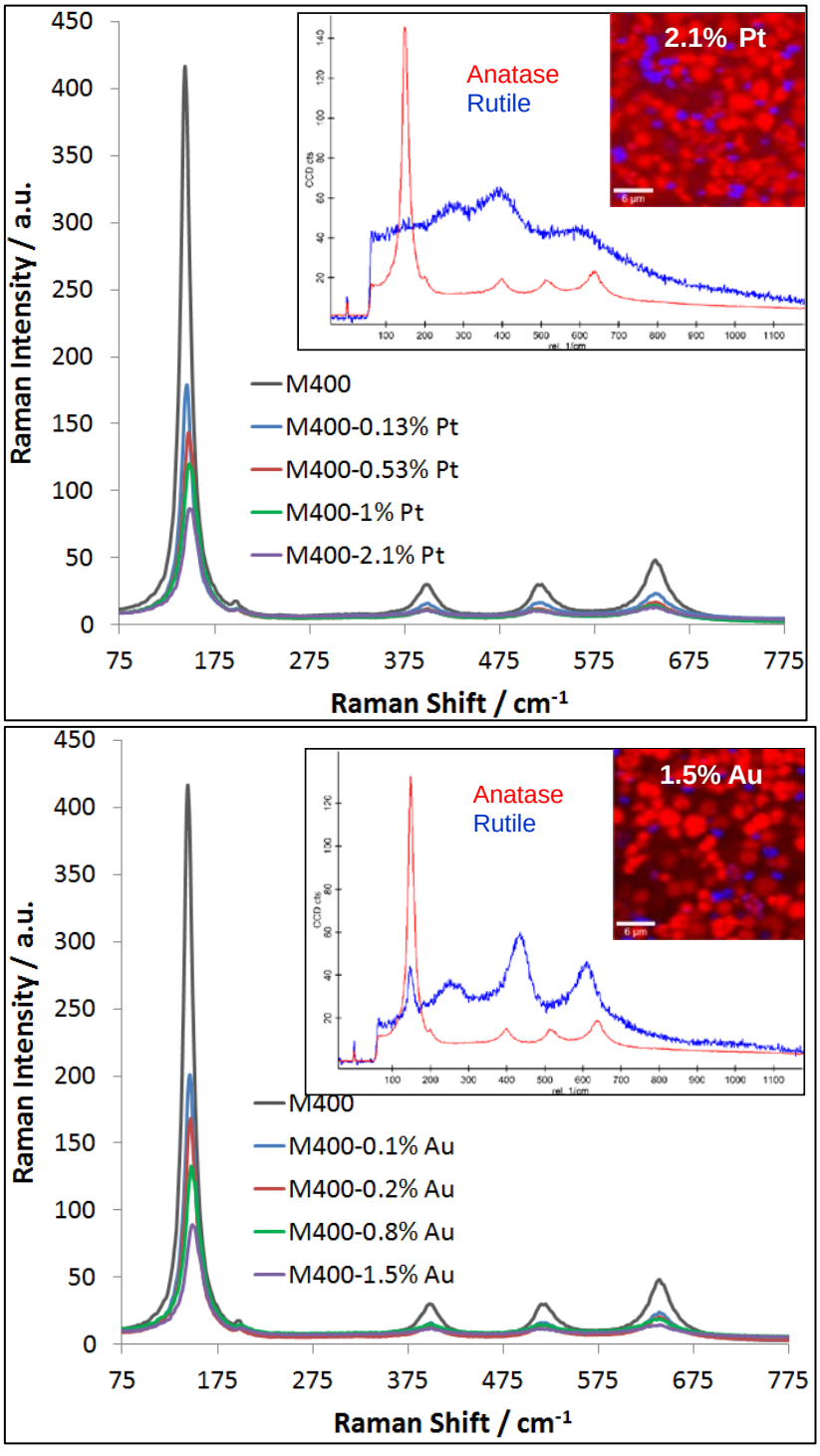

C)

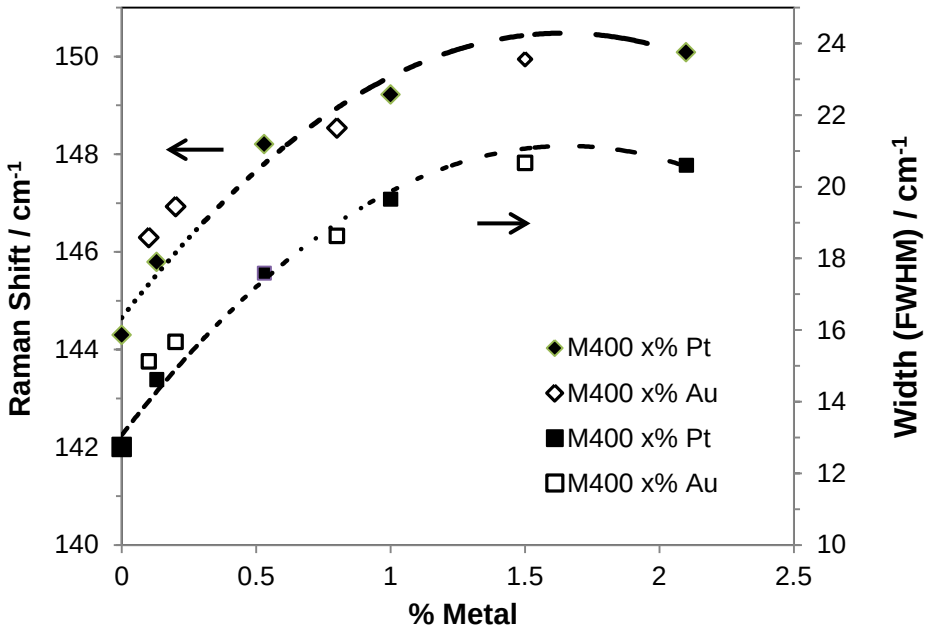

These effects and the decrease in the intensity of the bands may be due to various reasons, the most likely of which is the loss of stoichiometry through the formation of oxygen vacancies as a consequence of the photodeposition process [52]. Therefore, the deposition of metal particles does not completely eliminate the dissociative adsorption centres of the water and methanol and, in consequence, surface hydroxylation is maintained after metal photodeposition. This must be closely related to the micrometric size of these microsphere particles. It was also concluded from the Raman analysis that the particles were not completely covered with metal, not even at the highest percentages tested, as the TiO_2 was still observed. This was also seen in the EDX analysis (not shown), where it was noted that the Au and Pt deposits were not homogenous in all the sample.

The mechanism for the photocatalytic production of hydrogen with the Pt-modified TiO_2 catalysts [13, 26, 51, 53] (Scheme 1A) is such that, after photoexcitation of the TiO_2 particle, the methanol acts as a hole scavenger and the photoelectron migrates to the Pt nanoparticles:

$$e^- + Ti(IV)OH \longrightarrow Ti(III)OH^- \cdots \rightarrow\rightarrow Ti(III)OH / Pt^- \qquad (10)$$

where $Ti(III)OH/Pt^{-}$ represents the transfer of the electron from the hydroxylated surface trap of the TiO_2 to the Pt through the semiconductor-metal heterojunction. The Pt particles, as previously mentioned, would possibly preferentially occupy the oxygen vacancies [45], although they could also generate new vacancies according to the Raman signal analyses. This elimination and generation of vacancies could be a factor in the maximum hydrogen production being attained, in the case of the M400, at a low Pt load, 0.27wt%, as an increase in Pt load would entail a higher occupation of these centres which are the sites where the methanol adsorption takes place. That the photodeposited Pt preferentially occupies these centres is shown by the decrease in methanol adsorption with higher Pt loading. Once the methanol has been adsorbed and the hydrogen ion transferred to the medium, the latter is transported by the water to the Pt nanoparticles. Here, when it meets other hydrogen ions that can originate as the result of the direct oxidation of the water in the holes photoreduction takes place.

$$h^{+} + Ti\left(IV\right)OH_2 \longrightarrow Ti\left(IV\right) - {}^{\bullet}OH + H^{+} \tag{11}$$

As previously mentioned, and as is reflected in reactions (7) and (8), while there remain hydrogen atoms attached to the *C* of the alcohol group, hydrogen ions will continue to be generated by these reactions, transported to the Pt nanoparticles, and eventually reduced to hydrogen. This would explain the higher quantities of the intermediates, formaldehyde and formic acid, detected in liquid phase after the reaction compared to those detected in the tests undertaken with the unmodified photocatalysts.

Scheme 1. Mechanism of charge carriers for TiO_2 microspheres modified with Pt and Au.

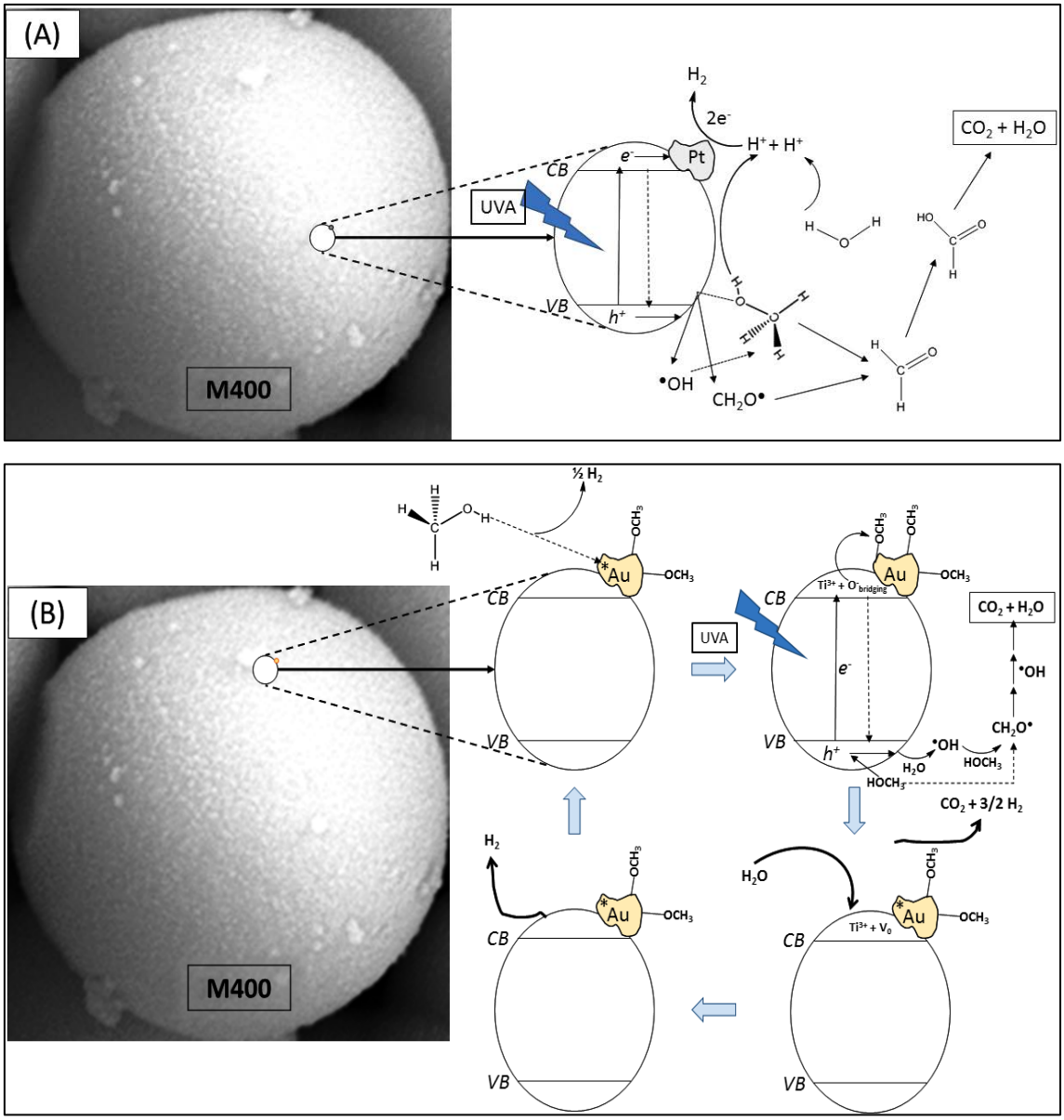

The different behaviour of this catalyst when loaded with Au appears to confirm a different reaction mechanism (Scheme 1B) to when it is loaded with Pt, as proposed by various authors for Au-modified TiO_2 [51, 53, 54]. The fundamental difference lies in the dissociative adsorption of the methanol in active sites on the metal, forming methoxy species adsorbed even in the absence of light and which are stable at ambient temperature:

$$CH_3OH\,(aq) + Au/TiO_2 \longrightarrow CH_3O - Au/TiO_2 + \frac{1}{2}H_2 \qquad (12)$$

Once the Au-modified M400 particle has been irradiated, the photodissociation of electron-hole pairs takes place and the strongly oxidising O^- species proposed by Bowker et al [54] oxidizes the methoxy group generating CO_2 and hydrogen and a free active site on the metal surface to be occupied by another methanol molecule. An oxygen vacancy is created on the TiO_2 surface which is regenerated by a water molecule and hydrogen is liberated. The process, following reaction (12), can be summarised in the following stages:

$$Ti^{4+}O^{2-} + h\nu \longrightarrow Ti^{3+} + O^- \quad (13)$$

$$CH_3O - Au/TiO_2 + O^- + Ti^{3+} \longrightarrow CO_2 + \frac{3}{2}H_2 + Au/TiO_2 + V_0^{2-} + Ti^{4+} \quad (14)$$

$$H_2O + Ti^{4+} + V_O^{2-} \longrightarrow Ti^{4+}O^{2-} + H_2 \quad (15)$$

Given the morphology of the TiO_2 microsphere calcined at 400°C, with appropriate specific area and porosity, ideal surface hydroxylation and a micrometric as opposed to nanometric particle size, it seems obvious that, as Au load is increased, up to 1.5%, the adsorption of methanol at the active metal sites will continue to be favoured as, hence, will hydrogen production. The detected intermediates, formaldehyde and formic acid, would seem to suggest that the possibility should not be discarded of adsorption of methanol in the photogenerated holes. Equally, the possibility should not be discarded that reaction (14), which reflects the oxidation of the *C* of the methoxy group adsorbed on the Au/TiO_2 surface, is not immediately completed to CO_2 but leads firstly to the formation of formaldehyde and its subsequent oxidation to formic acid.

Conclusions

The synthesised photocatalysts, with hierarchical structure and microsphere morphology, gave one of the highest hydrogen production rates reported to date in the literature for bare TiO_2 photocatalysts, 24.64 $\mu mol \cdot h^{-1}$, exceeding by 6-fold the production rate obtained with the commercial P25 catalyst. The photocatalytic activity of the unmodified microspheres in terms of hydrogen production appears to be closely correlated to structural parameters, surface hydroxylation and the number of shallow electron traps.

Modification through the surface incorporation of Au and Pt particles at respective percentages of 1.5% and 0.27% favoured the appearance of rutile phase, at trace level, detected by Raman spectroscopy and not XRD. In the presence of these metals,

hydrogen production rates increased by two orders of magnitude. In the case of Au, production increased with metal loading, reaching 1118 $\mu mol \cdot h^{-1}$ at 1.5wt%, while with the incorporation of Pt this rate was doubled with a metal content 6 times lower.

In the case of the Pt-modified microspheres, the presence of holes on the TiO_2 surface is required for adsorption of the sacrificial agent. The photodeposition of a high Pt load results in a decrease of available holes, a consequent decrease in methanol adsorption and, hence, a reduction in hydrogen production. This explains why the highest hydrogen production is attained with the M400-Pt catalysts at a low Pt load.

In the case of the Au-modified microspheres, a constant increase in hydrogen production was found as the Au percentage was increased. With the M400-Au photocatalyst, this could be related to a different mechanism of catalytic methanol photoreforming in the presence of Au as opposed to Pt, based, as some authors maintain, on the adsorption of the methanol on the Au particle. This allows greater availability for the adsorption of methanol other than in the photogenerated holes. However, oxygen vacancies need to be available to allow the water to regenerate the semiconductor surface. If the Au particles cover all the surface of the semiconductor or a significant part of it, hydrogen production will logically decrease or cease.

Acknowledgements

This work was supported by the Spanish Ministry of Science and Innovation through the project IPT-120000-2010-033 (GESHTOS). We would also like to thank the Spanish Ministry of Science and Innovation for the UNLP10-3E-726 infrastructure, co-financed with ERDF funds. T. Jardiel also acknowledges the financial support of the MAT2014-59210-JIN project of MINECO. M. Nereida Suárez would also like to thank the University of Las Palmas de Gran Canaria for its funding though the PhD Grant Program.

References

[1] Chen J, Huang Y, Zhang N, Zou H, Liu R, Tao C, Fan X, Wang ZL. Micro-cable structured textile for simultaneously harvesting solar and mechanical energy. Nature Energy 2016;1:16138-16148. https://doi.org/10.1038/nenergy.2016.138

[2] Zheng L, Cheng G, Chen J, Lin L, Wang J, Liu Y, Li H, Wang ZL. A Hybridized Power Panel to Simultaneously Generate Electricity from Sunlight, Raindrops, and

Wind around the Clock. Adv. Energy Mater. 2015;5:1501152. https://doi.org/10.1002/aenm.201501152

[3] Chen J, Yang J, Li Z, Fan X, Zi Y, Jing Q, Guo H, Wen Z, Pradel KC, Niu S, Wang ZL. Networks of Triboelectric Nanogenerators for Harvesting Water Wave Energy: A Potential Approach toward Blue Energy. ACS Nano 2015;9:3324-3331. https://doi.org/10.1021/acsnano.5b00534

[4] Kondarides DI, Verykios XE. Photocatalytic production of renewable hydrogen. In: Triantafyllidis KS, Lappas AA, Stöcker M, editors. The role of catalysis for the sustainable production of bio-fuels and bio-chemicals, The Netherlands: Elsevier; 2013, 495-527.

[5] Hosseini SE, Wahid MA. Hydrogen production from renewable and sustainable energy resources: Promising green energy carrier for clean development. Renew. Sust. Energ. Rev. 2016;57:850-66. https://doi.org/10.1016/j.rser.2015.12.112

[6] Zhang N, Chen J, Huang Y, Guo W, Yang J, Du J, Fan X, Tao C. A Wearable All-Solid Photovoltaic Textile. Mater. 2016;28:263-269. https://doi.org/ 10.1002/adma.201504137

[7] Zhang L, Zhang B, Chen J, Jin L, Deng W, Tang J, Zhang H, Pan H, Zhu M, Yang W, Wang ZL. Lawn Structured Triboelectric Nanogenerators for Scavenging Sweeping Wind Energy on Rooftops. Adv. Mater. 2016;28:1650-1656. https://doi.org/10.1002/adma.201504462

[8] Yilmaz F, Balta MT, Selbas R. A review of solar based hydrogen production methods. Renew. Sust. Energ. Rev. 2016;56:171-8. https://doi.org/10.1016/j.rser.2015.11.060

[9] Ismail AA, Bahnemann DW. Photochemical splitting of water for hydrogen production by photocatalysis: A review. Energy Mater. Sol. Cells 2014;128:85-101. https://doi.org/10.1016/j.solmat.2014.04.037.

[10] Colón G. Towards the hydrogen production by photocatalysis. Appl. Catal. A: Gen. 2016;518:48-59. https://doi.org/10.1016/j.apcata.2015.11.042

[11] Li X, Yu J, Low J, Fang Y, Xiao J, Chen X. Engineering heterogeneous semiconductors for solar water splitting. J. Mater. Chem. A. 2015;3:2485-2534. https://doi.org/10.1039/C4TA04461D

[12] Ortega Méndez JA, López CR, Pulido Melián E, González Díaz O, Doña Rodríguez JM, Fernández Hevia D, Macías M. Production of hydrogen by water photo-

splitting over commercial and synthesised Au/TiO_2 catalysts. Appl. Catal. B: Environ. 2014;147:439-52. https://doi.org/10.1016/j.apcatb.2013.09.029

[13] Pulido Melián E, López CR, Ortega Méndez A, González Díaz O, Suárez MN, Doña Rodríguez JM, Navío JA, Fernández Hevia D. Hydrogen production using Pt-loaded TiO_2 photocatalysts. Int. J. Hydrog. Energy 2013;38:11737-48. https://doi.org/10.1016/j.ijhydene.2013.07.006

[14] Wang B, Lu XY, Yu LK, Xuan J, Leung MKH, Guo H. Facile synthesis of TiO_2 hollow spheres composed of high percentage reactive facets for enhanced photocatalytic activity. CrystEngComm 2014;16:10046-55. https://doi.org/10.1039/C4CE00826J

[15] Zhu Z, Kao CT, Tang BH, Chang WC, Wu RJ. Efficient hydrogen production by photocatalytic water-splitting using Pt-doped TiO_2 hollow spheres under visible light. Ceram. Int. 2016;42:6749-54. https://doi.org/10.1016/j.ceramint.2016.01.047

[16] Wu D, Zhu F, Li J, Dong H, Li Q, Jiang K, Xu D. Monodisperse TiO_2 hierarchical hollow spheres assembled by nanospindles for dye-sensitized solar cells. J. Mater. Chem. 2012;22:11665-11671. https://doi.org/10.1039/C2JM30786C

[17] Wang Z, Wang ZC, Madhavi S, Lou XW. One-step synthesis of SnO_2 and TiO_2 hollow nanostructures with various shapes and their enhanced lithium storage properties. Chemistry 2012;18(24):7561-7567. https://doi.org/10.1002/chem.201103842.

[18] Gao M, Zhu L, Ong WL, Wanga J, Ho GW. Structural design of TiO_2-based photocatalyst for H_2 production and degradation applications. Catal. Sci. Technol., 2015;5:4703-26. https://doi.org/10.1039/C5CY00879D

[19] Yan K, Wu G, Jarvis C, Wen J, Chen A. Facile synthesis of porous microspheres composed of TiO_2 nanorods with high photocatalytic activity for hydrogen production. Appl. Catal. B: Environ. 148-149;2014:281-287. https://doi.org/10.1016/j.apcatb.2013.11.003

[20] Fan Z, Meng F, Zhang M, Wu Z, Sun Z, Li A. Solvothermal synthesis of hierarchical TiO_2 nanostructures with tunable morphology and enhanced photocatalytic activity. Appl. Surf. Sci. 360;2016:298-305. https://doi.org/10.1016/j.apsusc.2015.11.021

[21] Zhang P, Li A, Gong J. Hollow spherical titanium dioxide nanoparticles for energy and environmental applications. Particuology. 2015;22:13-23. https://doi.org/10.1016/j.partic.2015.03.001

[22] Yan K, Wu G. Titanium Dioxide Microsphere-Derived Materials for Solar Fuel Hydrogen Generation. ACS Sustainable Chem. Eng. 2015;3(5):779-791. https://doi.org/10.1021/acssuschemeng.5b00154

[23] Zheng Z, Huang B, Lu J, Qin X, Zhang X, Dai Y. Hierarchical TiO_2 Microspheres: Synergetic Effect of {001} and {101} Facets for Enhanced Photocatalytic Activity. Chemistry-A European Journal. 2011;17(52):15032-8. https://doi.org/10.1002/chem.201101466

[24] Yan K, Wu G, Jarvis C, Wen J, Chen A. Facile synthesis of porous microspheres composed of TiO_2 nanorods with high photocatalytic activity for hydrogen production. Appl. Catal. B: Environ. 2014;148-149:281-287. https://doi.org/10.1016/j.apcatb.2013.11.003.

[25] Jardiel T, Calatayud DG, Rodríguez M, Peiteado M, Fernández-Hevia D, Caballero AC. Facile synthesis of hierarchical anatase microspheres. J. Alloy. Comp. 2013;551:481-4. https://doi.org/10.1016/j.jallcom.2012.10.174

[26] Pulido Melián E, López CR, Santiago, Quesada-Cabrera R, Ortega Méndez JA, Doña Rodríguez JM, González Díaz O. Study of the photocatalytic activity of Pt-modified commercial TiO_2 for hydrogen production in the presence of common organic sacrificial agents. Appl. Catal. A: Gen. 2016;518:189-197. https://doi.org/10.1021/ef0400619

[27] Hufschmidt D, Bahnemann D, Testa JJ, Emilio CA, Litter MI. Enhancement of the photocatalytic activity of various TiO_2 materials by platinisation. J. Photochem. Photobiol. A: Chem. 2002;148:223-231. https://doi.org/10.1016/S1010-6030(02)00048-5

[28] Pulido Melián E, Suárez MN, Jardiel T, Doña Rodríguez JM, Caballero AC, Araña J, Calatayud DG, González Díaz O. Influence of nickel in the hydrogen production activity of TiO_2. Appl. Catal. B: Environ. 2014;152-153:192-201. https://doi.org/10.1016/j.apcatb.2014.01.039

[29] Kennedy ER, NIOSH Manual of Analytical Method (NMAM). Formaldehyde: Method 3500, 4th ed. Atlanta; 1994, Issue 2, p. 2-5.

[30] Kubelka P, Munk F. Ein Beitrag Zur Optik Der Farbanstriche. Zeitschrift für Technische Physik 1931;12:593-601.

[31] Weckhuysen BM, Schoonheydt RA. Recent progress in diffuse reflectance spectroscopy of supported metal oxide catalysts. Catal. Today 1999;49:441-51. https://doi.org/10.1016/S0920-5861(98)00458-1

[32] Tauc J. Optical properties and electronic structure of amorphous Ge and Si. Mat. Res. Bull. 1968;3:37-46.

[33] Liu Z, Zhang X, Nishimoto S, Jin, M, Tryk, DA, Murakami T, Fujishima A. Anatase TiO_2 nanoparticles on rutile TiO_2 nanorods: a heterogeneous nanostructure via layer-by-layer assembly. Langmuir 2007;23:10916-10919. https://doi.org/10.1021/la7018023

[34] Hurum DC, Agrios AG, Gray KA, Rajh T, Thurnauer MC. Explaining the enhanced photocatalytic activity of Degussa P25 mixed phase TiO_2 using EPR. J. Phys. Chem. B 2003;107:4545-4549. https://doi.org/10.1021/jp0273934

[35] Liu SW, Yu JG, Jaroniec M. Tunable photocatalytic selectivity of hollow TiO_2 microspheres composed of anatase polyhedra with exposed {001} facets. J Am Chem Soc 2010;132:11914-11916. https://doi.org/10.1021/ja105283s

[36] Du X, He JH, Zhao YQ. Facile preparation of F and N codoped pinecone-like titania hollow microparticles with visible light photocatalytic activity. J Phys Chem C 2009;113:14151-14158. https://doi.org/10.1021/jp9056175

[37] Wang JG, Yang Y, Huang ZH, Kang FY. Interfacial synthesis of mesoporous MnO_2/polyaniline hollow spheres and their application in electrochemical capacitors. J. Power Sources 2012;204:236-243. https://doi.org/10.1016/j.jpowsour.2011.12.057

[38] Pellow-Jarman MV, Hendra PJ, Lehnert RJ. The dependence of Raman signal intensity on particle size for crystal powders. Vibrational Spectroscopy 1996;12:257-261. https://doi.org/10.1016/0924-2031(96)00023-9.

[39] Pulido Melián E, López CR, Ortega Méndez A,González Díaz A, Suárez MN, Doña Rodríguez JM, Navío JA, Fernández Hevia D. Hydrogen production using Pt-loaded TiO_2 photocatalysts. Int. J. Hydrog. Energy 2013;38:11737-11748. https://doi.org/10.1016/j.ijhydene.2013.07.006

[40] Thompson TL, Yates JT. Surface science studies of the photoactivation of TiO_2 new photochemical processes. Chem. Rev. 2006;106:4428-4453. https://doi.org/10.1021/cr050172k.

[41] Szczepankiewicz SH, Colussi AJ, Hoffmann MR. Infrared spectra of photoinduced species on hydroxylated titania surfaces. J. Phys. Chem. B 2000;104:9842-9850. https://doi.org/10.1021/jp0007890.

[42] Panayotov D, Yates Jr. JT. Electron exchange on TiO_2–SiO_2 photocatalysts during O_2 and organic molecule adsorption – the role of adsorbate electrophilicity. Chem. Phys. Lett. 2003;381:154-162. https://doi.org/10.1016/j.cplett.2003.09.004.

[43] Dimitar A. Panayotov 1, John T. Yates Jr. n-Type doping of TiO_2 with atomic hydrogen-observation of the production of conduction band electrons by infrared spectroscopy. Chem. Phys. Lett. 2007;436:204–208. https://doi.org/10.1016/j.cplett.2007.01.039.

[44] Bahruji H, Bowker M, Davies PR, Pedrono F. New insights into the mechanism of photocatalytic reforming on Pd/TiO_2. Appl. Catal. B: Environ. 2011:107:205-9. https://dx.doi.org/10.1016/j.apcatb.2011.07.015.

[45] Chen T, Feng Z, Wu G, Shi J, Ma G, Ying P, Li C. Mechanistic studies of photocatalytic reaction of methanol for hydrogen production on Pt/TiO_2 by in situ Fourier transform IR and time-resolved IR spectroscopy. J. Phys. Chem. C 2007;111(22):8005-14. https://doi.org/10.1021/jp071022b.

[46] Dimitar A. Panayotov, Paul A. DeSario, Jeremy J. Pietron, Todd H. Brintlinger, Lindsey C. Szymczak, Debra R. Rolison. Ultraviolet and visible photochemistry of methanol at 3D mesoporous networks: TiO_2 and $Au{-}TiO_2$. J. Phys. Chem. C 2013;117:15035-49. https://dx.doi.org/10.1021/jp312583w.

[47] Litke A, Hensen EJM, Hofmann JP. Role of dissociatively adsorbed water on the formation of shallow trapped electrons in TiO_2 photocatalysts. J. Phys Chem C 2017;121:10153-62. https://doi.org/10.1021/acs.jpcc.7b01151.

[48] Davydov A. The Nature of Oxide Centers: Spectra of Oxide Surfaces. In: N. T. Sheppard editor. Molecular Spectroscopy of Oxide Catalyst Surfaces, John Wiley & Sons Ltd., 2003, 71-73.

[49] Davydov A. Surface Complexes of Organic Molecules. In: N. T. Sheppard editor. Molecular Spectroscopy of Oxide Catalyst Surfaces, John Wiley & Sons Ltd., 2003, 424.

[50] Busca G, Lamotte J, Lavalley JC, Lorenzelli V. FT-IR study of the adsorption and transformation of formaldehyde on oxide surfaces. J. Am. Chem. Soc. 1987;109(17):5197-202. https://doi.dx.org/10.1021/ja00251a025.

[51] Rossetti I, Hydrogen Production by Photoreforming of Renewable Substrates, International Scholarly Research Network (ISRN) Chemical Engineering. Volume 2012, ID 964936. https://dx.doi.org/10.5402/2012/964936.

[52] Šćepanović MJ, Grujić-Brojčin M, Dohčević-Mitrović Z, Popović ZV. Effects of confinement, strain and nonstoichiometry on Raman spectra of anatase TiO_2 nanopowders. Mater Sci Forum 2006;518:101-106. https://doi.org/10.4028/www.scientific.net/MSF.518.101

[53] Rosseler O, Shankar MV, Du MKL, Schmidlin L, Keller N, Keller V. Solar light photocatalytic hydrogen production from water over Pt and Au/TiO_2 (anatase/rutile) photocatalysts: influence of noble metal and porogen promotion. J. Catal. 2010;269(1):179-90. https://dx.doi.org/10.1016/j.jcat.2009.11.006.
[54] Bowker M, Millard L, Greaves J, James D, Soares J. Photocatalysis by Au nanoparticles: reforming of methanol. Gold Bulletin 2004;37(3-4):170-3. https://doi.org/10.1007/BF03215209.